




A backpack-based myeloid cell therapy for multiple sclerosis

Neha Kapate^{a,b,c} , Michael Dunne^{a,b}, Ninad Kumbhojkar^{a,b}, Supriya Prakash^{a,b}, Lily Li-Wen Wang^{a,b,c}, Amanda Graveline^b, Kyung Soo Park^{a,b}, Vineeth Chandran Suja^{a,b} , Juhee Goyal^a, John R. Clegg^{a,b,1} , and Samir Mitragotri^{a,b,2}

Edited by Chad Mirkin, Northwestern University, Evanston, IL; received December 19, 2022; accepted March 20, 2023

Multiple sclerosis (MS) is an incurable autoimmune disease and is currently treated by systemic immunosuppressants with off-target side effects. Although aberrant myeloid function is often observed in MS plaques in the central nervous system (CNS), the role of myeloid cells in therapeutic intervention is currently overlooked. Here, we developed a myeloid cell-based strategy to reduce the disease burden in experimental autoimmune encephalomyelitis (EAE), a mouse model of progressive MS. We developed monocyte-adhered microparticles (“backpacks”) for activating myeloid cell phenotype to an anti-inflammatory state through localized interleukin-4 and dexamethasone signals. We demonstrate that backpack-laden monocytes infiltrated into the inflamed CNS and modulated both the local and systemic immune responses. Within the CNS, backpack-carrying monocytes regulated both the infiltrating and tissue-resident myeloid cell compartments in the spinal cord for functions related to antigen presentation and reactive species production. Treatment with backpack-monocytes also decreased the level of systemic pro-inflammatory cytokines. Additionally, backpack-laden monocytes induced modulatory effects on T_H1 and T_H17 populations in the spinal cord and blood, demonstrating cross talk between the myeloid and lymphoid arms of disease. Backpack-carrying monocytes conferred therapeutic benefit in EAE mice, as quantified by improved motor function. The use of backpack-laden monocytes offers an antigen-free, biomaterial-based approach to precisely tune cell phenotype *in vivo*, demonstrating the utility of myeloid cells as a therapeutic modality and target.

Immunoengineering | CNS | myeloid | macrophages | phenotype

Multiple sclerosis (MS) is a currently incurable autoimmune disease characterized by inflammation and demyelination, leading to progressive neurodegeneration (1, 2). While adaptive immune cells are ultimately responsible for demyelination in MS (3), myeloid cells are known to play an important role in the initiation and exacerbation of MS (4). Myeloid cells constitute the largest population of central nervous system (CNS)-resident immune cells, comprising primarily of tissue-resident microglia and circulating monocytes that infiltrate and differentiate into macrophages (5). Not surprisingly, macrophages and microglia are the predominant inflammatory cells in active MS lesions (6–8). Myeloid cells also produce several inflammatory cytokines, free radicals, and other mediators that augment the inflammatory milieu, which in turn contributes to axonal injury (4, 9).

Current MS treatments are based largely on systemic immunomodulators, including interferon- β injections, oral glatiramer acetate, and oral fingolimod (1, 10, 11). These treatments are primarily aimed at reducing flares, rather than preventing disease, for relapsing MS, and are ineffective for progressive MS. Corticosteroids are also often used as a supplementary option for reduction of flares (12). All these treatments mediate their effect through systemic immunosuppression, with little to no direct impact at the target site due to the ineffective delivery of these drugs into the CNS (1, 2, 10). In particular, treatments for progressive MS are limited by lack of drug access to the compartmentalized innate immune response in the CNS (13). Current experimental therapies are dominated by systemically delivered small molecules and monoclonal antibodies, with a majority constituting currently approved immunomodulators for other indications or new dosing regimens. Some examples of new experimental therapeutic modalities include Bruton's tyrosine kinase inhibitors (evobrutinib, fenebrutinib, tolebrutinib), phosphodiesterase inhibitor (ibudilast), statins (Simvastatin), antisense oligonucleotide for CD49d (ATL1102), and allogeneic Epstein–Barr virus T cells (ATA188), all delivered systemically (14–16).

Despite their key role in the pathophysiology of MS, current treatments do not specifically target pro-inflammatory myeloid cells or make their use for modulating the disease. There is growing recognition, however, that the therapeutic activity of current MS therapies that target the adaptive immune system is actually indirectly mediated through myeloid cells (4, 17). Taking advantage of the ability of circulating monocytes to infiltrate into the CNS, here we report an anti-inflammatory myeloid cell therapy for the treatment of progressive

Significance

Multiple sclerosis (MS) is a currently incurable autoimmune disease with a complex disease pathology. Despite the key role of myeloid cells in the pathophysiology of MS, current treatments do not specifically target myeloid cells or directly make their use for modulating the disease. We propose that immunomodulatory monocytes, upon intravenous injection, can infiltrate into inflamed central nervous system and have the potential to mitigate disease progression. We control monocyte phenotype through cell surface-adhered particles (“backpacks”) loaded with interleukin-4 and dexamethasone. Treatment with backpack-laden monocytes elicited local and systemic immunomodulatory effects, culminating in improved motor functions in experimental autoimmune encephalomyelitis mice. The results reported here demonstrate the possibility of myeloid cells as a therapy and drug target in MS.

Competing interest statement: The authors have organizational affiliations to disclose. S.M. is a board member of Hitch Bio and is a shareholder of Hitch Bio. Neha Kapate, Ninad Kumbhojkar, S.P., L.-L.W.W., and S.M. are inventors on patent applications related to the technology described in the manuscript (owned and managed by Harvard University).

This article is a PNAS Direct Submission.

Copyright © 2023 the Author(s). Published by PNAS. This article is distributed under [Creative Commons Attribution-NonCommercial-NoDerivatives License 4.0 \(CC BY-NC-ND\)](https://creativecommons.org/licenses/by-nc-nd/4.0/).

¹Present address: Stephenson School of Biomedical Engineering, University of Oklahoma, Norman, OK 73019.

²To whom correspondence may be addressed. Email: mitragotri@seas.harvard.edu.

This article contains supporting information online at <https://www.pnas.org/lookup/suppl/doi:10.1073/pnas.2221535120/-/DCSupplemental>.

Published April 19, 2023.

MS. Specifically, we propose that immunomodulatory monocytes, upon intravenous injection, can infiltrate into the inflamed CNS and elicit an anti-inflammatory phenotype to mitigate disease progression. To control the therapeutic phenotype of injected cells in vivo, disk-shaped particles (“backpacks”), containing interleukin-4 (IL-4) and dexamethasone, were designed, synthesized, and attached to monocytes. Backpack-laden monocytes exhibited infiltration into the CNS of mice with experimental autoimmune encephalomyelitis (EAE) and modulated both the local and systemic immune responses, thereby improving disease burden.

Results

Design and Characterization of Backpack-Monocytes. We designed disk-shaped, microparticles (backpacks) that carry drug molecules and reproducibly adhere to primary monocytes. The backpacks were prepared from poly-lactic-co-glycolide (PLGA) and poly(vinyl alcohol) (PVA) by spin coating in a layer-by-layer fashion, allowing for design modularity. The backpacks consisted of a layer of PLGA/dexamethasone, a layer of PVA/heparin/IL-4, and a final layer of PLGA/dexamethasone (Fig. 1*A*). The PLGA layers were composed of a 2:1 polymer blend of PLGA and PLGA-PEG-maleimide. Heparin was used in the PVA layer to stabilize IL-4 and improve loading (18) (*SI Appendix, Fig. S1A*). After microcontact printing, the backpacks were resuspended and functionalized with CD45 F(ab') to functional maleimide groups on the backpack surface via thiol-maleimide click chemistry. The backpacks displayed an average diameter of $7.75 \pm 0.25 \mu\text{m}$, an average thickness of $505.73 \pm 43.1 \text{ nm}$, and an average stiffness of $7.37 \pm 0.15 \text{ GPa}$, as determined by atomic force microscopy (AFM) (*SI Appendix, Fig. S1B*). The backpacks retained their morphology when resuspended in aqueous solution (*SI Appendix, Fig. S1C*). Backpack-monocyte complexes were prepared by mixing primary monocytes and backpacks at optimized incubation parameters (Fig. 1*B*). A backpack:monocyte ratio of 3:1 during incubation was determined to promote substantial adhesion of anti-CD45-functionalized backpacks to monocytes, while minimizing cell aggregation (*SI Appendix, Fig. S2A*). Anti-CD45 F(ab')-functionalized backpacks exhibited excellent adhesion to murine bone-marrow-derived monocytes, with 60.5% of monocytes attached to at least one backpack, compared to 12.9% for unmodified backpacks (Fig. 1*C*). Backpack adhesion to monocytes was further confirmed and visualized using confocal microscopy (Fig. 1*D* and *SI Appendix, Fig. S2B*). We also confirmed that the backpacks efficiently attached to primary human blood-derived monocytes (*SI Appendix, Fig. S2C*). To verify whether the backpacks remained adhered to the monocytes under physiological disturbances, the backpack-carrying monocytes were exposed to physiologically relevant shear stresses (19). Across increasing shear conditions (2, 6, and 20 Pa), the backpacks remained adhered to the monocytes (Fig. 1*E*). Furthermore, the backpacks did not adversely impact the viability of carrier monocytes (Fig. 1*F*). In fact, drug-loaded backpacks led to improved viability compared to untreated monocytes and monocytes treated with free drugs for 72 h (*SI Appendix, Fig. S2D*). This could be due to monocytes being exposed to gradual drug release, compared to a bolus dose of free drug at once.

Dexamethasone and IL-4 were chosen as therapeutic payloads due to their potency in stimulating anti-inflammatory functions, such as tissue repair, phagocytosis, and reactive species processing [associated with biomarkers CD206 (11) and arginase-1 (Arg1) (20)] while dampening pro-inflammatory functions, such as antigen presentation and costimulation [associated with biomarkers MHCII (21) and CD80 (11)]. By investigating the expression of

these biomarkers, we found that dexamethasone and IL-4 acted synergistically on macrophages and achieved a unique phenotype that was only observed upon exposure to both drugs (*SI Appendix, Fig. S2E*). The potent effect of IL-4 and dexamethasone on macrophages makes them excellent candidates for prolonged cell stimulation using backpacks. Backpacks released dexamethasone and IL-4 for at least 5 d (Fig. 1*G*). The total drug loading was $37.42 \pm 1.68 \mu\text{g}$ dexamethasone per 10^6 backpacks and $183.1 \pm 15.2 \text{ ng}$ IL-4 per 10^6 backpacks (Fig. 1*G*).

Backpacks Induce Anti-inflammatory Myeloid Phenotype. IL-4 and dexamethasone backpacks induced a strong anti-inflammatory myeloid phenotype, as indicated by reduced expression of pro-inflammatory markers [MHCII, CD80, CD86, inducible nitric oxide synthase (iNOS)] and increased expression of anti-inflammatory markers (CD206, Arg1, IL-10) after backpack-laden monocytes were cultured and allowed to differentiate for 48 h (Fig. 2*A* and *SI Appendix, Fig. S3*). Compared to control monocytes, backpack-carrying monocytes demonstrated significantly decreased MHCII expression (0.42-fold), CD80 expression (0.22-fold), and iNOS expression (0.81-fold). Backpack-carrying monocytes also demonstrated significantly increased CD206 expression (5.60-fold), Arg1 expression (12.5-fold), and IL-10 expression (1.89-fold). Monocyte activation by backpacks was durable, as seen by phenotype maintenance when backpack-carrying monocytes were cultured in pro-inflammatory media (*SI Appendix, Fig. S4*), which is expected to resemble in vivo conditions. To characterize the effect of backpacks on the local biochemical environment, cytokine production from backpack-carrying monocytes was assessed 24 h after backpack attachment (Fig. 2*B*). Backpack-monocytes demonstrated significantly decreased secretion of pro-inflammatory cytokines (i.e., IL-6 and TNF α) and significantly increased secretion of relevant anti-inflammatory and wound-healing cytokines (i.e., IL-10 and TGF β).

As monocytes respond to chemotactic gradients to migrate from circulation to sites of inflammation, it is vital that backpack-monocytes retain chemokine receptor expression. Chemokine receptors CCR2 and CX3CR1 have been implicated in the extravasation and transmigration of monocytes under inflammatory conditions, including MS (22, 23). Our data suggest that CCR2 and CX3CR1 expression of monocytes was not affected by the backpack attachment (Fig. 2*C*). In fact, a significant increase in CCR2 and CX3CR1 expression was observed in the backpack-containing subset of backpack-monocytes (*SI Appendix, Fig. S5A*). Monocytes with blank backpacks also displayed increased CCR2 and CX3CR1 expression, demonstrating that the backpack itself may impact the cell (*SI Appendix, Fig. S5B*). Further, backpack attachment did not influence transendothelial migration of murine monocytes, as assessed ex vivo (Fig. 2*D*). Similar observations were made for primary human monocytes (*SI Appendix, Fig. S5C*). Backpack-laden monocytes maintained their ability to differentiate into macrophages, as quantified by F4/80 expression after 48 h (Fig. 2*E*).

Backpack-Carrying Monocytes Traffic and Accumulate in the CNS. EAE is a murine model of progressive MS that shares many clinical, histopathological, and immunological characteristics with MS (24, 25) and hence was chosen to assess the therapeutic efficacy of backpack-carrying monocytes. Intravenously injected backpack-carrying monocytes, administered at the onset of disease signs, accumulated in the CNS of EAE mice (Fig. 3*A–C*). In fact, the percent relative dose of backpack-monocytes that infiltrated the CNS after 24 h was 1.59%, which was significantly greater than in the case of monocytes alone, 0.96% (Fig. 3*C*). The overall

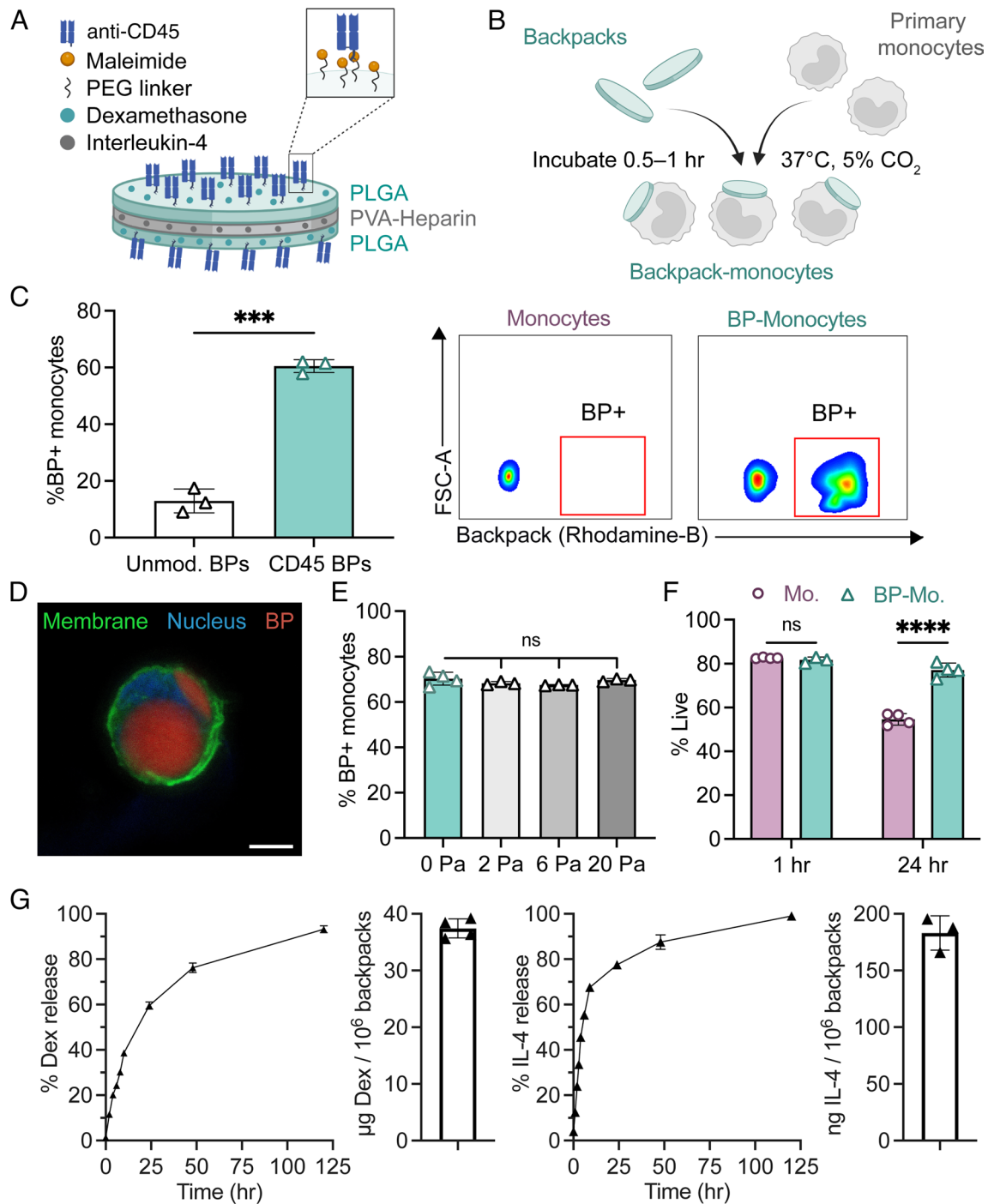


Fig. 1. Design and characterization of backpack-carrying monocytes. (A) Schematic of backpack (BP) design, including dexamethasone and IL-4 loading and anti-CD45 F(ab') functionalization. (B) Schematic of backpack attachment to primary monocytes. (C) Percentage of monocytes with >1 backpack (determined by flow cytometry); mean \pm SD ($n = 3$). Representative flow cytometry gating of control monocytes vs. backpack-adhered monocytes. (D) Confocal micrograph of monocyte (membrane: green, nucleus: blue) with backpack (red). (Scale bar, 5 μ m.) (E) Percentage of monocytes with backpacks attached following shear studies (determined by flow cytometry); mean \pm SD ($n = 3$ to 4). (F) Percentage of live cells at 1 h and 24 h for monocytes (Mo.) and backpack-monocytes (BP-Mo.) (determined by flow cytometry); mean \pm SD ($n = 3$ to 4). (G, Left) Release and loading of dexamethasone over time, quantified by HPLC. Dexamethasone loading was determined by degrading backpacks postfabrication via chemical dissolution and quantifying dexamethasone content. Right, release and loading of IL-4 over time, quantified by ELISA. IL-4 loading calculated by cumulative release from backpacks after 14 d, at which point apparent drug release ceased. Mean \pm SD ($n = 3$ to 4). For C, data were analyzed by two-tailed Student's t test, $***P < 0.001$. For E, data were analyzed by one-way ANOVA with Tukey's HSD test; ns, not significant. For F, data were analyzed by two-way ANOVA with Sidak's correction. $****P < 0.0001$.

organ accumulation at 24 h of backpack-monocytes was quantified via *in vivo* imaging system (IVIS) (SI Appendix, Fig. S6). We observed that backpack-monocytes persist in the CNS of EAE for up to 5 d (Fig. 3D). Although the greatest proportion of backpack-monocytes were present in the brain and spinal cord 24 h after administration, backpack-monocytes could be visualized in the CNS 2 d and 5 d after administration (Fig. 3D and SI Appendix,

Fig. S7). The overall organ accumulation at 2 and 5 d after administration was also quantified (SI Appendix, Fig. S8).

By analyzing single-cell suspensions of the CNS, we found that backpack-carrying monocytes exhibited higher infiltration into the spinal cord (120,756 cells/g organ) compared to control monocytes (50,240 cells/g) (Fig. 3E). No significant difference was observed between the number of control monocytes (6,901

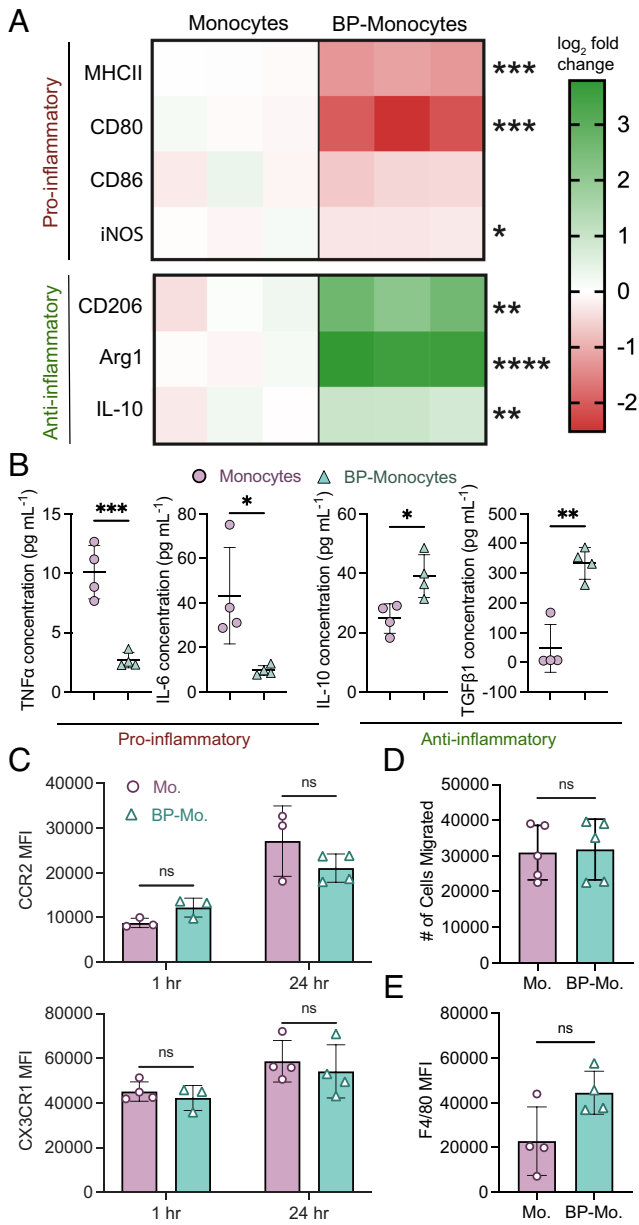


Fig. 2. Backpacks induce anti-inflammatory phenotype in differentiating monocytes. (A) Monocytes or backpack-monocytes were cultured for 48 h and analyzed for expression of pro-inflammatory (MHCII, CD80, CD86, and iNOS) and anti-inflammatory (CD206, Arg1, IL-10) markers. Heatmap columns show data from individual replicates ($n = 3$), reported as log₂ fold change in expression compared to the average value of the monocyte group. Raw data are in *SI Appendix, Fig. S3*. (B) Cytokine excretion from monocytes or backpack-monocytes after 24 h; mean \pm SD ($n = 3$). (C) Chemokine receptor expression of monocytes (Mo.) and backpack-monocytes (BP-Mo.) at 1 h and 24 h, quantified by flow cytometry; mean \pm SD ($n = 3$ to 4). (D) Migration was assessed using a Transwell assay, with endothelial cells seeded on 5 μ m inserts, and media containing 10 ng/mL CCL2 added to the lower chamber. A total of 200k monocytes or backpack-monocytes were added into the upper chamber. The number of monocytes or backpack-monocytes in the lower chamber after 24 h was counted; mean \pm SD ($n = 5$). (E) Monocytes or backpack-monocytes were plated and differentiated for 48 h. F4/80 expression was quantified via flow cytometry; mean \pm SD ($n = 4$). For A, B, D, and E, data were analyzed by two-tailed Student's *t* test; ns, not significant, * $P < 0.05$, ** $P < 0.01$, *** $P < 0.001$, **** $P < 0.0001$. For C, data were analyzed by two-way ANOVA with Sidak's correction; ns, not significant.

cells/g organ) and backpack-carrying monocytes (11,455 cells/g) in the brain (Fig. 3E). Blood concentrations of control monocytes (2,351 cells/100 μ L blood) and backpack-carrying monocytes (2,479 cells/100 μ L blood) were also comparable (Fig. 3E). Importantly, when free backpacks were administered, only 339

backpacks/g organ and 122 backpacks/g extravasated into the spinal cord and brain, respectively, which was 356-fold and 93-fold lower than the quantity of backpack-monocytes that infiltrated into the respective CNS components (*SI Appendix, Fig. S9*).

The backpacks remained attached to the carrier monocytes as monocytes infiltrated into the CNS (Fig. 3F). Backpack adhesion stability, quantified as the proportion of monocytes tracked in vivo carrying backpacks compared to monocytes carrying backpacks pre-injection, was 79.9% for the brain and 81.1% for the spinal cord. Fluorescence imaging confirmed that monocytes and backpacks were colocalized in the spinal cord parenchyma (Fig. 3B).

Backpack-Monocytes Impact Immune Cell Profiles in the CNS. Treatment with backpack-carrying monocytes elicited changes in the myeloid cell profile of the CNS, compared to the control groups (Fig. 4 A and B). Although the abundances of general immune cells were similar across groups (*SI Appendix, Fig. S10*), among the infiltrating myeloid cells in the spinal cord, there was a significant decrease in iNOS⁺-infiltrating myeloid cells compared to saline and control monocytes with blank backpacks (Fig. 4 A and B, *i*). A significant increase in Arg1⁺-infiltrating myeloid cells was also observed for the backpack-carrying monocytes compared to the other groups (Fig. 4 B, *i*). Among the resident myeloid cells of the spinal cord, there was a significant decrease in MHCII^{high} and CD80⁺ resident myeloid cells for backpack-carrying monocytes compared to saline (Fig. 4 B, *ii*). These changes correspond to decreased inflammatory hallmarks typically associated with pro-inflammatory myeloid cells. A significant increase was observed in IFN β levels, an EAE-resolving mediator, and a significant decrease was observed in IL-6 and IFN γ levels, EAE-exacerbating mediators after treatment with backpack-carrying monocytes (Fig. 4C) (26, 27). Additional organ cytokine analysis can be found in *SI Appendix (SI Appendix, Fig. S11)*. Further analysis of the systemic immune response revealed significant decreases in TNF α , IL-17A, and IL-12p70 levels in the serum, common pro-inflammatory mediators (Fig. 4D) (28). Expanded cytokine analysis in the serum is included in *SI Appendix, Fig. S12*. Finally, we assessed cross talk between the myeloid and lymphoid arms of disease by analyzing T cell subsets, as pro-inflammatory myeloid cells can induce T_H1 and T_H17 responses, two drivers of disease pathology (12). On day 15, within the spinal cord, there was a significant decrease in IFN γ ⁺CD4⁺ T cells in the backpack-monocyte-treated group, signifying a decrease in T_H1 cells, and a significant increase in ROR γ T⁺CD4⁺ T cells within the control monocyte group, signifying an increase in T_H17 cells (Fig. 4E). This effect on the adaptive immune system was maintained at day 25, where a decrease in IL-17A⁺ CD4⁺ T cells in the blood was seen after treatment with backpack-monocytes, demonstrating a decrease in pathogenic T_H17 cells (Fig. 4F). No significant differences were seen in the general immune cell population at this time point in the CNS or blood (*SI Appendix, Fig. S13*). Overall, treatment with backpack-monocytes elicited changes in the immune milieu by reducing inflammation through local anti-inflammatory activation of myeloid cells and secretion of inflammation-resolving mediators. Treatment with drug-loaded backpacks alone, the relevant drug dosage control, demonstrated negligible effects on the local and systemic immune environment.

Backpack-Monocytes Confer Therapeutic Benefit in a Mouse Model of Progressive MS. Treatment with backpack-carrying monocytes, dosed therapeutically at the onset of disease signs, led to a significant decrease in disease score over time compared to monocytes alone or saline (Fig. 5 A and B). Treatment with backpack-monocytes reversed disease progression to a presentation of limp tail, compared to complete hind limb paralysis in the

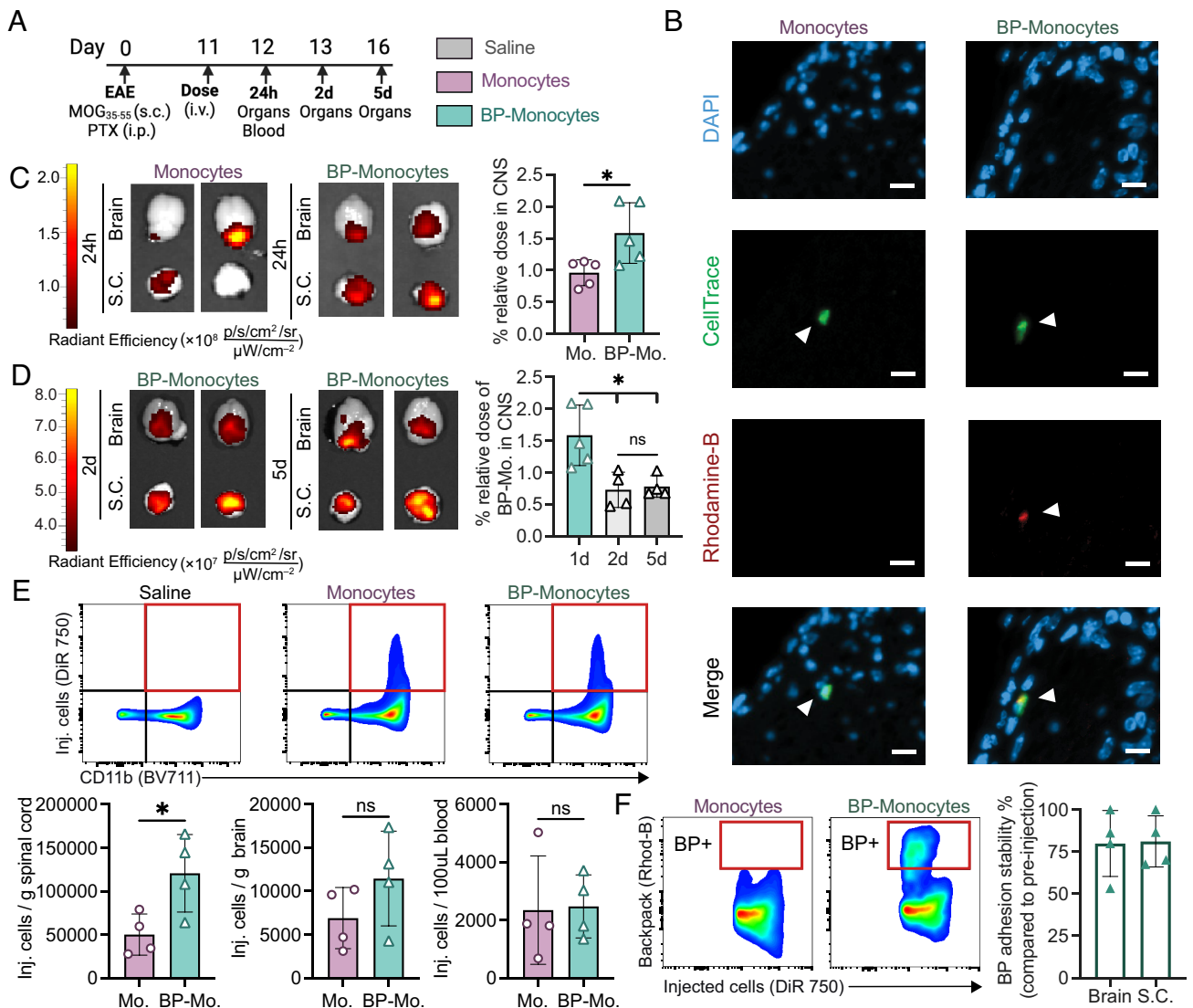


Fig. 3. Backpack-carrying monocytes migrate to the CNS of EAE mice. EAE was induced in female C57BL/6J mice. (A) The mice were treated with 3×10^6 monocytes or backpack-monocytes or saline (i.v. tail vein) at the onset of clinical signs on day 11, with the adoptively transferred cells stained with DiR 750 or CellTrace Far Red. On days 12, 13, and 16, the CNS and blood were harvested for ex vivo imaging and single-cell suspension processing. (B) Fluorescence imaging of lumbar spinal cord stained for DAPI (nucleus, blue), CellTrace (adoptively transferred cells, green), and rhodamine-B [backpacks (BP), red]. (Scale bar represents 10 μ m.) (C) Representative IVIS of brain and spinal cord (S.C.) displaying DiR 750 signal 24 h after monocyte (Mo.) or BP-monocyte (BP-Mo.) administration. Fluorescence quantification of relative dose accumulated in the CNS (cumulative brain and spinal cord signal) for monocytes and backpack-monocytes; mean \pm SD (n = 5). (D) Representative IVIS images of brain and spinal cord displaying DiR 750 signal 2 d and 5 d hours after BP-monocyte (BP-Mo.) administration. Fluorescence quantification of relative dose accumulated in the CNS (cumulative brain and spinal cord signal); mean \pm SD (n = 4). (E) Representative gating for tracking injected cells (DiR 750) after 24 h in the single-cell suspension of the spinal cord; flow cytometry quantification of adoptively transferred cells in the single-cell suspensions of the spinal cord, brain, and blood; mean \pm SD (n = 4). (F) Representative flow cytometry gating and quantification for backpack attachment to adoptively transferred cells in spinal cord single-cell suspension. Adhesion stability is quantified as percent of adoptively transferred monocytes with a backpack adhered as compared to pre-injected backpack-monocyte adhesion; mean \pm SD (n = 5). For C, D, E, data were analyzed using two-tailed Student's t test; ns, not significant, * $P < 0.05$.

control groups, and overall diminished cumulative score (Fig. 5 B and C). Furthermore, we report a significant decrease in maximum disease score for the backpack-monocyte group compared to monocytes or saline (Fig. 5D). When comparing day of onset of maximum score, the maximum score occurred at a similar time across groups (Fig. 5E), demonstrating that treatment with backpack-monocytes dampened disease severity, rather than delayed disease progression. Histopathology analyses of the lumbar spinal cord on day 25 showed reduced inflammatory immune cell infiltration in mice treated with backpack-monocytes, compared to treatment with monocytes or saline (Fig. 5 F and G). Treatment with backpack-monocytes resulted in a survival benefit, where all mice dosed with backpack-monocytes survived to the end of the study (Fig. 5H). The biocompatibility of backpack-monocytes was assessed by body weight, hematological analysis, blood

chemistry, and blinded histological evaluation of major organs. Hematological analysis and blood chemistry data suggested that backpack-monocytes did not lead to significant changes in the tested markers as compared to the untreated group (SI Appendix, Fig. S14). Similarly, H&E analysis of the major organs was normal for the treated groups compared to untreated (SI Appendix, Fig. S15). Given the limitations of dosing (29), half-life (30), and inability to cross the blood–brain barrier (31–33), free drug combination was not tested in the survival study.

Discussion

Myeloid cell therapy presents an untapped opportunity for the treatment of MS. Delivery of monocytes alone, however, is not a viable option since phenotype-controlling supporting therapies,

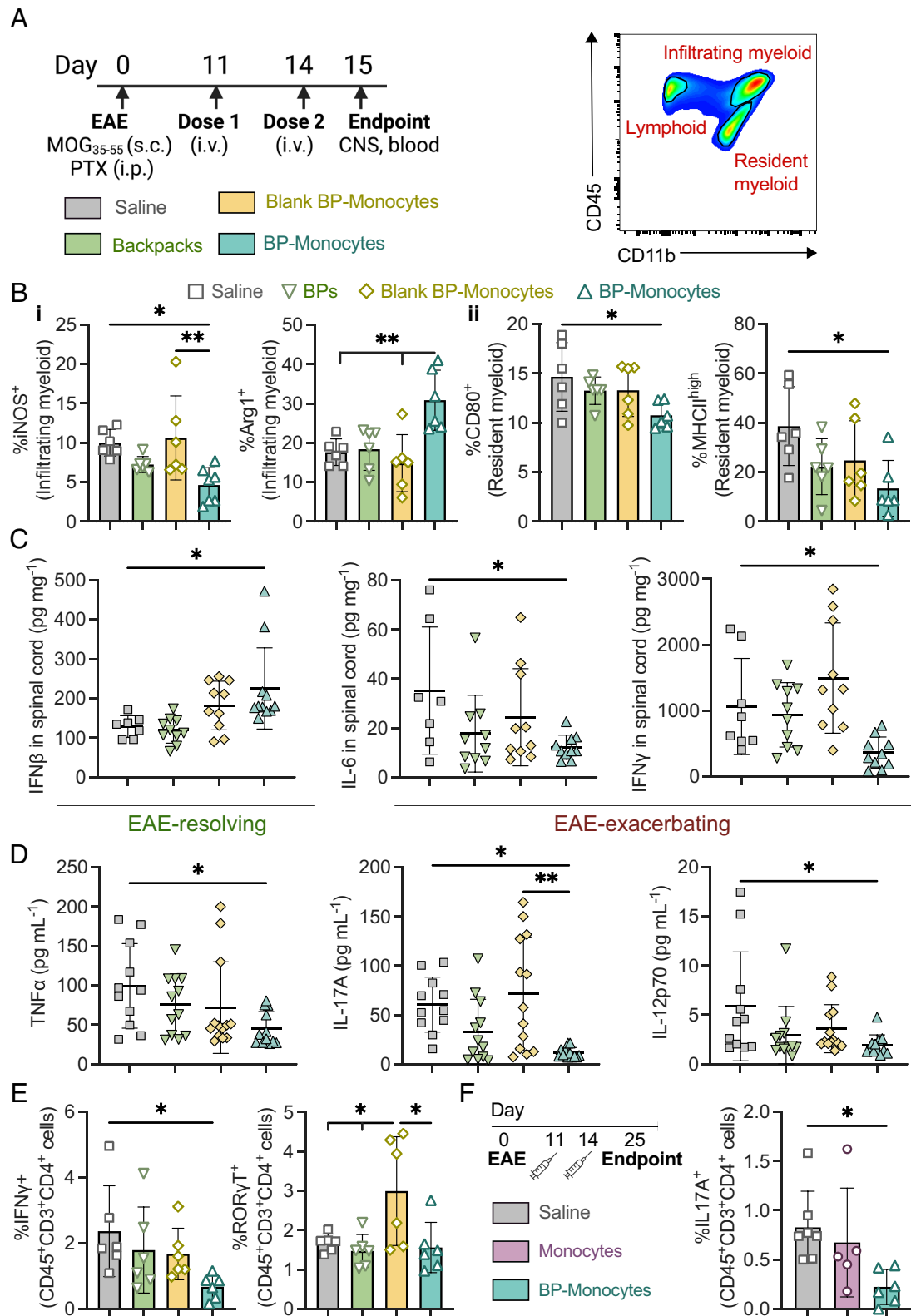


Fig. 4. Backpack-laden monocytes modulate the CNS immune microenvironment. EAE was induced in female C57BL/6 mice. (A) The mice were treated with 3×10^6 backpacks (BPs), blank backpack-monocytes, backpack-monocytes, or saline on days 11 and 14 (i.v. tail vein). On day 15, blood and CNS were harvested. Representative depiction of flow cytometry gating for distinguishing tissue-resident and tissue-infiltrating myeloid cells. (B) The spinal cord was processed into single-cell suspensions and analyzed via flow cytometry to profile the (i) infiltrating and (ii) tissue-resident myeloid cell populations; mean \pm SD (n = 5). (C) Concentrations of anti-/pro-inflammatory mediators from spinal cord homogenate at day 15; mean \pm SD (n = 10 to 11). (D) Serum concentrations of pro-inflammatory mediators at day 15; mean \pm SD (n = 10 to 11). (E) IFN γ ⁺ and ROR γ T⁺ CD4 T cell populations in the spinal cord at day 15; mean \pm SD (n = 5). (F) EAE was induced, and mice were treated with 3×10^6 monocytes or BP-monocytes or saline at days 11 and 14. At day 25, the IL-17A⁺ T_H17 population of the blood was analyzed; mean \pm SD (n = 7). For B–F, data were analyzed using one-way ANOVA with Tukey's HSD test; ns, not significant, * P < 0.05, ** P < 0.01.

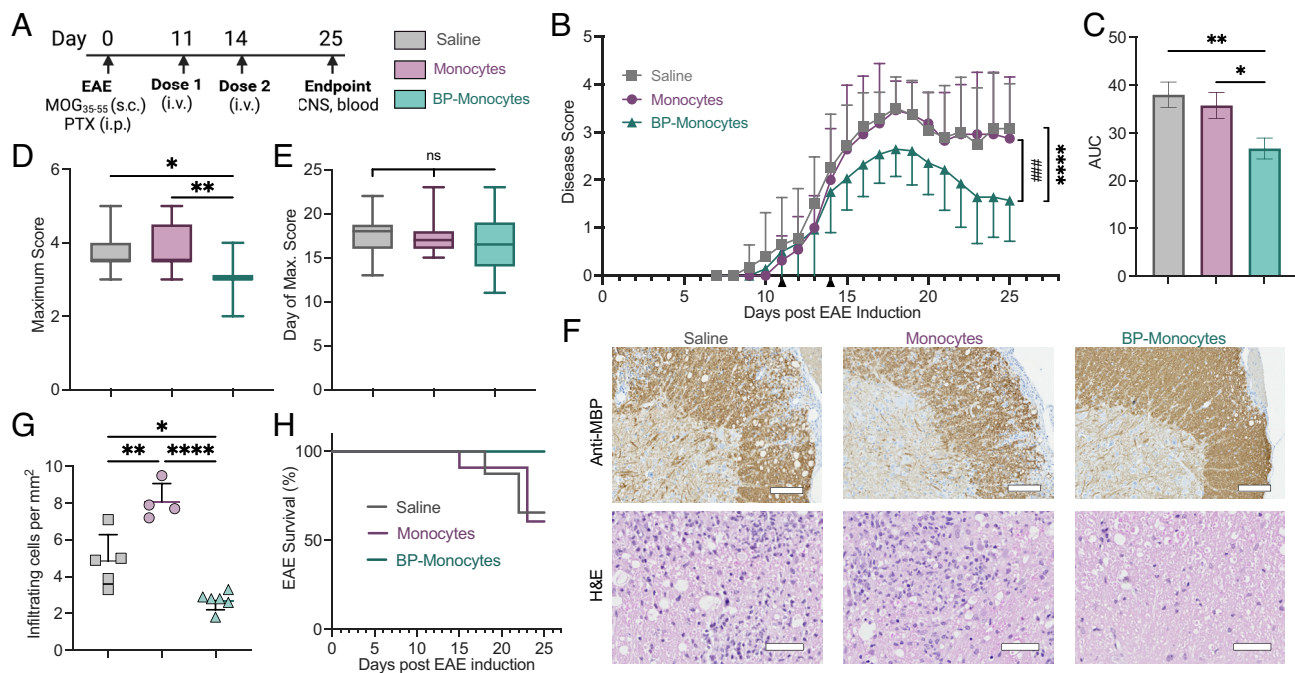


Fig. 5. Backpack-monocytes are therapeutically effective. EAE was induced in female C57BL/6J mice. (A) The mice were treated with monocytes, backpack-laden monocytes (BP-monocytes), or saline on days 11 and 14 (i.v. tail vein). The mice were scored until day 25. (B) Disease score over time; mean \pm SE (n = 11 to 14). (C) Area under the curve (AUC) of disease score; mean \pm SD (n = 11 to 14). (D) Maximum disease score; mean \pm SD (n = 11 to 14). (E) Day of onset of maximum score; mean \pm SD (n = 11 to 14). (F) Representative antimyelin basic protein (MBP) staining, revealing areas of demyelination, and hematoxylin and eosin (H&E) staining, revealing inflammatory infiltrates, for lumbar spinal cord sections of mice from B (n = 5). Anti-MBP scale bar represents 100 μ m. H&E scale bar represents 50 μ m. (G) Inflammatory infiltrating cells per mm² from lumbar spinal cord sections from B; mean \pm SD (n = 4 to 6). (H) EAE survival percentage from mice in B. (n = 11 to 14). For B, data were analyzed by two-way ANOVA with Bonferroni's multiple comparison; *****P* < 0.0001 comparing saline and backpack-monocytes; ###*P* < 0.001 comparing monocytes and backpack-monocytes. For C and E, data were analyzed using one-way ANOVA with Tukey's HSD test; ns, not significant, **P* < 0.05, ***P* < 0.01.

such as cytokines, are necessary to maintain immune cell function. Systemic delivery of supporting therapies often results in off-target side effects (34). Cell-adhering backpacks address this challenge by providing a high local drug dose to control cell phenotype *in vivo*, while minimizing systemic drug dose. We designed and characterized backpacks adhered to monocytes for modulating myeloid cell phenotype into an anti-inflammatory state. Backpacks were loaded with IL-4 and dexamethasone, which were chosen for their potency, in combination, for stimulating anti-inflammatory, regulatory functions [i.e., phagocytic activity (35), oligodendrogenesis (36)] while dampening pro-inflammatory functions [i.e., antigen presentation (37), cytokine secretion (38)] to achieve a unique, therapeutically relevant cell phenotype. As IL-4 and dexamethasone are both pleiotropic molecules, loading them into cell-associated backpacks allows for localization of drug activity to the desired therapeutic site with minimal systemic exposure.

Backpacks persistently activated myeloid cells to an anti-inflammatory, regulatory phenotype. In EAE, CNS myeloid cells, including tissue-infiltrating macrophages and resident microglia, demonstrate up-regulated antigen presentation, reflecting interactions with CNS-invading T cells (5). Backpack-carrying monocytes demonstrated significant decreases in MHCII and CD80 expression, correlating to decreased antigen presentation and costimulation. Backpack-carrying monocytes demonstrated significant decrease in iNOS expression and increase in Arg1 expression, correlating to processing of reactive oxygen and nitrogen species, mediators of tissue injury and neurodegeneration (39). Finally, backpack-carrying monocytes demonstrated significant increases in CD206 expression, relevant for phagocytosis and processing of myelin debris, and IL-10, relevant for pleiotropic wound-healing effects. These cellular phenotype changes were accompanied by increased secretion of anti-inflammatory cytokines (i.e., IL-10,

TGF β 1) and decreased secretion of pro-inflammatory cytokines (i.e., IL-6, TNF α), allowing backpack-laden monocytes to modulate the lesion microenvironment.

In EAE mice, backpack-carrying monocytes migrated to the inflamed CNS with superior trafficking abilities compared to control monocytes. Significantly more backpack-carrying monocytes extravasated into the spinal cord compared to monocytes, which could be attributed to inflammation being initiated in the spinal cord in EAE (1). We hypothesize that the improved trafficking by backpack-monocytes is due to increased chemokine receptor expression of backpack-containing monocytes, increasing the propensity of backpack-carrying monocytes to respond to soluble chemokine cues and migrate to inflamed tissues.

Backpack-carrying monocytes conferred therapeutic benefit in EAE mice, as quantified by improved motor function. Treatment with backpack-carrying monocytes was administered at the onset of disease signs, which is more clinically relevant than studies with prophylactic treatment. The magnitude of measured therapeutic benefit reported here with only 2 doses is on par with reported therapeutic treatment with the standards of care fingolimod (dosed daily) and methylprednisolone (dosed every other day) (40). Since the monocyte therapy reported here focuses on the myeloid arm of the disease, it leads to the possibility that treating both arms of the disease in conjunction may lead to synergistic benefit. Indeed, many current MS therapies that target the adaptive immune system, primarily T cells and B cells, also affect myeloid cells, which are being recognized for their contribution to efficacy of these treatments (4).

Studies reported here show that treatment with backpack-carrying monocytes modulated both the local and systemic immune responses. Within the CNS, backpack-monocytes regulated both the resident and infiltrating myeloid cell compartments in the brain and spinal

cord. This is necessary, as macrophages and microglia are the predominant inflammatory cells in active MS lesions (6–8). Our approach is based on findings which suggest that the initial pro-inflammatory polarization of myeloid phagocytes needs to be prevented when treating inflammatory CNS diseases (41). After treatment with backpack-monocytes, resident myeloid cells demonstrated reduced antigen presentation and costimulation, which may promote antigen-specific suppression of autoreactive T cells. Infiltrating myeloid cells demonstrated increased Arg1 expression and decreased iNOS expression, reminiscent of the relevant myeloid phenotype during disease remission (42). Systemically, there was a decrease in relevant pro-inflammatory cytokines in the serum (28). Additionally, we observed a cross talk by the myeloid and lymphoid branches of the disease, evidenced by effects on T_{H1} and T_{H17} populations, important drivers of disease pathology. As bidirectional communication between T cells and myeloid cells can shape effector responses (3, 12, 13), these studies demonstrate the pleiotropic effects of myeloid cell therapy for curtailing the inflammatory milieu.

Overall, the studies reported here demonstrate a myeloid cell-based strategy to improve disease outcome in a mouse model of progressive MS. The use of backpack-monocytes offers a biomaterials approach to precisely modulate cell phenotype by providing prolonged cues to persist cellular phenotype *in vivo*. Currently, there are well-established methods for harvesting autologous monocytes from patients, involving leukapheresis and rapid monocyte purification, that take less than 3 h (43–45). Importantly, the use of backpacks is antigen free and does not require genetic engineering. These are vital considerations for translatability, given lack of knowledge regarding the antigens for MS initiation and poor success of antigen-based approaches in the clinic, along with regulatory and manufacturing hurdles for genetically modified cells. Disease treatment could be improved in combination with other medications that target the adaptive immune system, such as fingolimod, which sequesters lymphocytes in the lymph nodes. Backpacks also provide the opportunity to overcome biological barriers to deliver therapeutic agents to target tissues, including the brain (46, 47). Taking into consideration the significant role of myeloid cells in disease initiation and progression, our findings support the potential of myeloid cells as a therapeutic modality and target in MS.

Materials and Methods

Materials. PLGA resomer 502H, dexamethasone, PVA, heparin RPMI 1640 media, fetal bovine serum, penicillin and streptomycin, phosphate-buffered saline (PBS), UltraComp eBeads compensation beads, and LIVE/DEAD Blue dye were purchased from Sigma-Aldrich. PLGA-rhodamine was obtained from PolySciTech Akina. Recombinant murine IL-4, recombinant murine macrophage colony-stimulating factor, and murine IL-4 ELISA kits were obtained from PeproTech. Sylgard 184 Silicone Elastomer kit was purchased from Dow. DiR 750 Fluorescent Cell Labeling Dye was obtained from PerkinElmer. MOG₃₅₋₅₅/CFA Emulsion kits for EAE induction were obtained from Hooke Laboratories. Debris removal solution and tissue dissociation kits were obtained from Miltenyi Biotec. Cell staining buffer and Legendplex Mouse Inflammation Panel and Mouse Macrophage/Microglial Panel kits were purchased from BioLegend. All fluorescent probe-conjugated antibodies for immune cell staining were purchased from BioLegend, Invitrogen, or R&D Systems. Cell fixation/permeabilization kits were obtained from BD Biosciences.

Animals. Female C57BL/6J mice (6 to 11 wks of age) were purchased from Charles River Laboratories and Jackson Laboratories. All animal experiments were performed according to approved protocols by the Institutional Animal Care and Use Committee (IACUC) of the Faculty of Arts and Sciences, Harvard University, and the IACUC of the Longwood Medical Area, Harvard University.

Backpack Fabrication. Polydimethylsiloxane (PDMS) templates were prepared as described previously (48). Briefly, silicon wafers were fabricated with patterned photoresist in an array of 8 μ m holes. PDMS mixed in a 10:1 base

to crosslinker ratio from the Sylgard 184 kit was poured onto silicon wafers in Petri dishes. The PDMS was degassed and cured at 65 °C overnight and cut away from the silicon wafers. A solution of 80 mg/mL PLGA and 15 mg/mL dexamethasone in acetone was prepared, with a 2:1 ratio of PLGA (7 to 17 kDa; Resomer 502 H) and PLGA-PEG-maleimide (10 kDa PLGA; 5 kDa PEG). For fluorescently labeled backpacks, PLGA-rhodamine B was incorporated at a ratio of 100:1 fluorescent to nonfluorescent PLGA. A volume of 220 μ L PLGA solution was spin coated onto each PDMS quadrant at 2,000 rpm for 35 s (at a 200 rpm/s ramp). Quadrants were plasma-ashed with O₂ for 60 s. A solution of 0.5 wt% PVA (146 to 186 kDa, 99 + % hydrolyzed) and 0.5 wt% heparin in PBS was prepared with IL-4 (25 μ g/mL). Immediately after plasma treatment, 50 μ L PVA/IL-4 solution was spread onto each quadrant. The quadrants were dried in a desiccator and then a second PLGA layer was deposited using the same procedure as the first. The backpacks were then stamped onto PVA-coated dishes by microcontact printing, as described previously (48). For blank backpacks, dexamethasone was omitted from the PLGA layers and IL-4 was omitted from the PVA layer. To collect backpacks, PVA-coated dishes were washed twice with 3 mL PBS. The solution was filtered through 20 μ m cell strainers, centrifuged at 2,000 g for 5 min, and then incubated with a solution of anti-CD45 F(ab') for 15 min to functionalize the backpacks. Anti-CD45 F(ab') fabrication process is described in [SI Appendix, Extended Methods](#). The backpacks were washed, pelleted, and resuspended in media of choice.

Backpack Characterization. To quantify drug release, backpacks were harvested from dishes and resuspended in RPMI + 0.1% BSA. The backpacks were incubated at 37 °C while rotating, and supernatant samples were taken at various time points. IL-4 release was quantified via ELISA and dexamethasone release was quantified via HPLC-MS, as described in [SI Appendix, Extended Methods](#). AFM (JPK NanoWizard, Bruker) was used to characterize the topology and stiffness of backpacks as described in [SI Appendix, Extended Methods](#).

Primary Monocyte Culture. Bone marrow cells were harvested by flushing the femurs and tibias of donor mice. The collected cells were filtered through 40 μ m cell strainers and centrifuged at 350 g for 7.5 min. Then, the bone marrow cells were resuspended in RPMI supplemented with 20 ng/mL M-CSF and plated at a density of 1×10^6 cells/mL in 6-well ultra-low attachment plates for differentiation into monocytes (49, 50). For studies with human monocytes, primary blood-derived monocytes were purchased from STEMCELL.

Preparation and Characterization of Backpack-Monocytes. Monocytes were harvested from culture, counted, and seeded in 50 μ L aliquots with 1×10^6 cells per well in a U-bottom 96-well plate. Backpacks were harvested and counted and added at a 3:1 backpack:cell ratio in 50 μ L aliquots. The monocytes and backpacks were incubated for 30 to 60 min at 37 °C, 5% CO₂ to allow attachment to occur. Then, the backpack-monocytes were harvested from the wells, pelleted at 300 g for 5 min, and resuspended in media of choice for subsequent use. Backpack adhesion was quantified via flow cytometry (Cytek Aurora) and confocal microscopy (Zeiss OIC LSM 900). For viability studies, backpack-monocytes were stained using LIVE/DEAD Blue (BioLegend) at 1 h (after backpack-monocyte preparation) and 24 h and analyzed via flow cytometry (Cytek Aurora). For shear studies, backpack-monocytes were loaded in a 1-mL syringe fitted with a 27-g blunt capillary needle (McMaster Carr #75165A688, 75165A763). The syringe was fixed on a syringe pump and dispensed with predetermined flow rates to subject backpack-monocytes to hydrodynamic shear stresses. The backpack-monocytes were subsequently quantified for attachment by flow cytometry. For migration studies, human umbilical vein endothelial cells (EA.hy926) were seeded on 5 μ m Transwell inserts, and media containing 10 ng/mL CCL2 was added to the lower chamber. A total of 200k monocytes or backpack-monocytes were added into the upper chamber. The number of monocytes or backpack-monocytes in the lower chamber after 24 h was counted.

In Vitro Phenotyping of Backpack-Monocytes. Monocytes or backpack-monocytes were prepared and cultured in nontissue culture-treated 24-well plates with 200,000 cells suspended in 750 μ L of growth media or growth media supplemented with 2 ng/mL IFN γ . To determine activation status and viability, the cells were cultured for 48 h; harvested; blocked with CD16/CD32 (BioLegend); and stained using LIVE/DEAD Blue (BioLegend), anti-F4/80-BV510 (BioLegend), anti-CD11b-BV785 (BioLegend), anti-CD80-Pe-Cy5 (BioLegend), anti-MHCII-Spark Blue

550 (BioLegend), anti-CD86-BV605 (BioLegend), and anti-CD206-AlexaFluor700 (BioLegend) antibodies. Samples were then fixed and permeabilized and stained using anti-Arg1-eFluor 450 (Invitrogen), anti-IL-10-APC-Cy7 (BioLegend), anti-iNOS-PE-Cy7 (Invitrogen), and anti-IFN γ -AlexaFluor647 (Invitrogen) antibodies. To determine chemokine receptor expression, backpack-monocytes or monocytes were cultured in 500 μ L of growth media at 100,000 cells per well in nontissue culture-treated 48-well plate. At 1 h and 24 h, cells were harvested; blocked with CD16/CD32 (BioLegend); and stained using LIVE/DEAD Blue (BioLegend), F4/80-BV510 (BioLegend), CD11b-BV711 (BioLegend), Ly6C-Pacific Blue (BioLegend), CCR2-FITC (BioLegend), and CX3CR1-APC (BioLegend) antibodies. Cytek Aurora analyzer was used, and data were analyzed with FlowJo V10. To determine cytokine excretion, monocytes or backpack-monocytes were seeded at 200k cells per well in non-tissue culture-treated U-bottom 96-well plates. After 24 h, the plate was centrifuged, and the supernatant was harvested. LEGENDplex™ Mouse Inflammation Panel (13-plex) and LEGENDplex™ Mouse Macrophage/Microglia Panel (13-plex) were used to assay the supernatant samples, following vendor instructions.

EAE Model Establishment. EAE was induced in female C57BL/6J mice (Jackson Laboratories) at 9 to 14 wk using the EK-2110 kit (Hooke Laboratories), with myelin oligodendrocyte glycoprotein 35-55 (MOG₃₅₋₅₅) and Complete Freund's Adjuvant emulsion and pertussis toxin injections as described in *SI Appendix, Extended Methods*. EAE severity was assessed using an established disease score rubric (51). Scoring was performed by an investigator blinded to the treatment groups. Mice were randomly assigned to different experimental treatments.

Biodistribution Study. Female C57BL6 mice were induced with EAE. Eleven days after EAE induction, when mice began showing clinical signs, 3×10^6 monocytes, backpacks, or backpack-monocytes were administered intravenously via tail vein. The backpacks were labeled with rhodamine and the monocytes were labeled with CellTrace Far Red (ThermoFisher) or IVISense DiR 750 (PerkinElmer) depending on the readout. Twenty-four hours, 2 d, or 5 d after administration, blood was drawn, and the mice were killed and perfused with saline. For a subset of the mice, the spinal columns were extracted, fixed in formalin for tissue sectioning, and submitted to Hooke Laboratories (Lawrence, MA) for sectioning and DAPI staining of the spinal cord. Tissue sections were imaged with Zeiss Axioscan. For a subset, the major organs, including brain, spinal cord, lungs, heart, liver, spleen, and kidneys, were extracted, and imaged by in vivo imaging system (PerkinElmer IVIS Spectrum). For the final subset of mice, the brain and spinal cord were harvested and digested into single-cell suspension as described in *SI Appendix*. To track the injected cells in the CNS, the single-cell suspensions were blocked with anti-CD16/CD32 antibody (BioLegend) and stained using LIVE/DEAD Blue (BioLegend), anti-CD11b-BV711 (BioLegend), and anti-CD45-FITC (BioLegend) antibodies. Cytek Aurora analyzer was used, and data were analyzed with FlowJo V10.

Characterization of Immune Responses Induced by Backpack-Monocytes. Female C57BL6 mice were induced with EAE. Eleven days after EAE induction, when mice began showing clinical signs, 3×10^6 backpacks, backpack-monocytes, monocytes with blank backpacks, or saline was administered intravenously via tail vein. Monocytes with empty backpacks were used because it has been shown that backpacks alone can affect the carrier cell (*SI Appendix, Fig. S5B*) (48). A second dose was administered 3 d later. Twenty-four hours after the second dose, the mice were perfused with saline and killed. The blood, brain, and spinal cord were harvested and processed into single-cell suspensions (*SI Appendix*). The samples were blocked with anti-CD16/CD32 (BioLegend), stained with LIVE/DEAD Blue (BioLegend), stained for surface markers, fixed and permeabilized, and stained for intracellular markers, as detailed in *SI Appendix, Extended Methods*. Cytek Aurora analyzer was used, and data were analyzed with FlowJo V10. Infiltrating myeloid cells and resident myeloid cells were defined based on differential CD45 expression for CD11b⁺ cells (CD45^{high}CD11b⁺ for resident

myeloid cells, CD45^{low}CD11b⁺ for infiltrating myeloid cells) (52, 53). Serum and organ suspension supernatant were collected, assayed with LEGENDplex™ Mouse Inflammation Panel (13-plex) and LEGENDplex™ Mouse Macrophage/Microglia Panel (13-plex), and analyzed with the Cytek Aurora.

Therapeutic Efficacy of Backpack-Monocytes. Female C57BL6 mice were induced with EAE. Eleven days after EAE induction, when mice began showing clinical signs, and 14 d after induction, 3×10^6 monocytes, backpack-monocytes, or saline was administered intravenously via tail vein. Body weight and clinical score were monitored for 25 d by an investigator blinded to the treatment groups. On day 25, blood was drawn and mice were perfused with saline, killed, and major organs were harvested. For a portion of the mice, the brain, spinal cord, and blood were digested to yield a single-cell suspension for flow cytometry analysis. A portion of the blood was saved for serum processing. The organ suspension supernatant was also saved. These samples were assayed with LEGENDplex™ Mouse Inflammation Panel (13-plex) and LEGENDplex™ Mouse Macrophage/Microglia Panel (13-plex) and analyzed with the Cytek Aurora. Hematoxylin and eosin (H&E) staining was performed on the non-CNS major organs (Harvard Medical School Rodent Histology Core Facility). For a portion of the mice, the spinal column was extracted and submitted to Hooke Laboratories (Lawrence, MA) for H&E and MBP staining of serial sections of the lumbar, thoracic, and cervical spinal cord. Tissue sections were imaged with Zeiss Axioscan. Immune cell infiltration was measured using QuPath v0.3.2 (54). Eight circular regions of interest, each equal to 23,000 μ m², were drawn on each H&E-stained image. The positive cell count analysis tool was used to measure the number of eosin-stained cells in the regions of interest. All analyses were conducted blind to the treatment administered. Blood and serum samples were submitted to IDEXX BioAnalytics for hematological and serum chemistry analysis.

Statistical Analysis. All statistical analyses were carried out using GraphPad Prism 8 software. As described in figure captions, unpaired Student's *t* test and one-way or two-way ANOVA with Tukey's HSD (honestly significant difference) test were used to determine significance. The *n* and *P* values are indicated in the legends. Flow cytometry analyses were carried out using FlowJo V10.

Data, Materials, and Software Availability. All relevant data and methods are reported in the manuscript. Please refer to *SI Appendix* for additional information on material characterization, mechanistic analysis, and biodistribution.

ACKNOWLEDGMENTS. We acknowledge Prof. Jennifer Guerriero, Dr. Jayoung Kim, Dr. Yongsheng Gao, Dr. Kolade Adebawale, and Alex Gottlieb for helpful scientific discussions. We also thank Andyna Vernet, Melinda Sanchez, and Sarai Bardales of the Wyss Institute for assistance with EAE mouse studies. N. Kapate was supported by the NSF Graduate Research Fellowship under Grant no. 1122374. We acknowledge Wyss Institute of Biologically Inspired Engineering and John A. Paulson School of Engineering at Harvard University for support. We acknowledge the Harvard Center for Biological Imaging; the Allston Science and Engineering Complex's Molecular and Cellular Biology Core; and Harvard University Center for Nanoscale Systems, a member of the National Nanotechnology-Coordinated Infrastructure Network supported by NSF ECCS-2025158. We also thank the Dana-Farber/Harvard Cancer Center in Boston, MA, for the use of the Rodent Histopathology Core and its histological section preparation service. We acknowledge the use of <https://www.biorender.com> in creating schematics.

Author affiliations: ^aJohn A. Paulson School of Engineering & Applied Sciences, Harvard University, Allston, MA 02134; ^bWyss Institute for Biologically Inspired Engineering, Boston, MA 02115; and ^cHarvard-MIT Division of Health Sciences and Technology, Massachusetts Institute of Technology, Cambridge, MA 02139

Author contributions: N. Kapate and S.M. designed research; N. Kapate, M.D., N. Kumbhojkar, S.P., L.L.-W.W., A.G., K.S.P., V.C.S., J.G., and J.R.C. performed research; N. Kapate analyzed data; and N. Kapate and S.M. wrote the paper.

1. C. A. Dendrou, L. Fugger, M. A. Friese, Immunopathology of multiple sclerosis. *Nat. Rev. Immunol.* **15**, 545–558 (2015).
2. M. T. Wallin *et al.*, The prevalence of MS in the United States. *Neurology* **92**, e1029–e1040 (2019).
3. K. E. Atfield, L. T. Jensen, M. Kaufmann, M. A. Friese, L. Fugger, The immunology of multiple sclerosis. *Nat. Rev. Immunol.* **22**, 1–17 (2022).
4. M. K. Mishra, V. Wee Yong, Myeloid cells—targets of medication in multiple sclerosis. *Nat. Rev. Neurol.* **12**, 539–551 (2016). [10.1038/nrneuro.2016.110](https://doi.org/10.1038/nrneuro.2016.110).

5. D. Mrdjen *et al.*, High-dimensional single-cell mapping of central nervous system immune cells reveals distinct myeloid subsets in health, aging, and disease. *Immunity* **48**, 380–395.e6 (2018).
6. C. Lucchinetti *et al.*, Heterogeneity of multiple sclerosis lesions: Implications for the pathogenesis of demyelination. *Ann. Neurol.* **47**, 707–717 (2001). [https://doi.org/10.1002/1531-8249\(200006\)47:6<707::AID-ANA3>3.0.CO;2-Q](https://doi.org/10.1002/1531-8249(200006)47:6<707::AID-ANA3>3.0.CO;2-Q).
7. L. W. Prineas *et al.*, Immunopathology of secondary-progressive multiple sclerosis. *Ann. Neurol.* **50**, 646–657 (2001).

8. O. W. Howell *et al.*, Activated microglia mediate axoglial disruption that contributes to axonal injury in multiple sclerosis. *J. Neuropathol. Exp. Neurol.* **69**, 1017–1033 (2010).
9. M. Strachan-Whaley, S. Rivest, V. W. Yong, Interactions between microglia and T cells in multiple sclerosis pathobiology. *J. Interferon Cytokine Res.* **34**, 615–622 (2014).
10. A. J. Thompson, S. E. Baranzini, J. Geurts, B. Hemmer, O. Ciccarelli, Multiple sclerosis. *Lancet* **391**, 1622–1636 (2018).
11. W. He, N. Kapate, C. W. Shields, S. Mitragotri, Drug delivery to macrophages: A review of targeting drugs and drug carriers to macrophages for inflammatory diseases. *Adv. Drug Deliv. Rev.* **165–166**, 15–40 (2019), [10.1016/j.addr.2019.12.001](https://doi.org/10.1016/j.addr.2019.12.001).
12. M. Filippi *et al.*, Multiple sclerosis. *Nat. Rev. Dis. Prim.* **4**, 1–27 (2018).
13. C. Baecher-Allan, B. J. Kaskow, H. L. Weiner, Multiple sclerosis: Mechanisms and immunotherapy. *Neuron* **97**, 742–768 (2018).
14. National Multiple Sclerosis Society, Clinical Trials Receiving Funding from the National MS Society. <https://www.nationalmssociety.org/getattachment/Research/Research-News-Progress/Clinical-Trials-in-MS/Clinical-Trials-Receiving-Funding.pdf?lang=en-US>. Accessed 2 April 2023.
15. MS Society, Explore treatments in trials. <https://www.msosociety.org.uk/research/explore-our-research/emerging-research-and-treatments/explore-treatments-in-trials>. Accessed 2 April 2023.
16. Y. Zhang, A. Salter, E. Wallström, G. Cutter, O. Stüve, Evolution of clinical trials in multiple sclerosis. *Ther. Adv. Neurol. Disord.* **12**, 1756286419826547 (2019).
17. K. Biber, T. Möller, E. Boddeke, M. Prinz, Central nervous system myeloid cells as drug targets: Current status and translational challenges. *Nat. Rev. Drug Discov.* **15**, 110–124 (2016).
18. L. Schirmer, P. Atallah, C. Werner, U. Freudenberg, StarPEG-heparin hydrogels to protect and sustainably deliver IL-4. *Adv. Healthc. Mater.* **5**, 3157–3164 (2016).
19. C. Mondadori *et al.*, Advanced microfluidic models of cancer and immune cell extravasation: A systematic review of the literature. *Front. Bioeng. Biotechnol.* **8**, 907 (2020).
20. A. D. Greenhalgh *et al.*, Arginase-1 is expressed exclusively by infiltrating myeloid cells in CNS injury and disease. *Brain. Behav. Immun.* **56**, 61–67 (2016).
21. V. Steimle, C. A. Siegrist, A. Mottet, B. Lisowska-Grospierre, B. Mach, Regulation of MHC class II expression by interferon-gamma mediated by the transactivator gene CIITA. *Science* **265**, 106–109 (1994).
22. H. X. Chu *et al.*, Role of CCR2 in inflammatory conditions of the central nervous system. *J. Cereb. Blood Flow Metab.* **34**, 1425–1429 (2014).
23. S. Rivest, CX3CR1 in multiple sclerosis. *Oncotarget* **6**, 19946 (2015).
24. T. M. Rivers, D. H. Sprunt, G. P. Berry, Observations on attempts to produce acute disseminated encephalomyelitis in monkeys. *J. Exp. Med.* **58**, 39–52 (1933).
25. J. M. Fletcher, S. J. Lalor, C. M. Sweeney, N. Tubridy, K. H. G. Mills, T cells in multiple sclerosis and experimental autoimmune encephalomyelitis. *Clin. Exp. Immunol.* **162**, 1–11 (2010).
26. M. Kocur *et al.*, IFN β secreted by microglia mediates clearance of myelin debris in CNS autoimmunity. *Acta Neuropathol. Commun.* **3**, 20 (2015).
27. Z. Jiang, J. X. Jiang, G. X. Zhang, Macrophages: A double-edged sword in experimental autoimmune encephalomyelitis. *Immunol. Lett.* **160**, 17 (2014).
28. A. J. Jahan-Abad *et al.*, Serum pro-inflammatory and anti-inflammatory cytokines and the pathogenesis of experimental autoimmune encephalomyelitis. *Neuropathology* **40**, 84–92 (2020).
29. J. Nam, T. K. Koppinen, M. H. Voutilainen, MANF is neuroprotective in early stages of EAE, and elevated in spinal white matter by treatment with dexamethasone. *Front. Cell. Neurosci.* **15**, 1–13 (2021).
30. P. J. Conlon, S. Tyler, K. H. Grabstein, P. Morrissey, Interleukin-4 (B-cell stimulatory factor-1) augments the in vivo generation of cytotoxic cells in immunosuppressed animals. *Biotechnol. Ther.* **1**, 31–41.
31. B. A. Duffy, K. P. Chun, D. Ma, M. F. Lythgoe, R. C. Scott, Dexamethasone exacerbates cerebral edema and brain injury following lithium-pilocarpine induced status epilepticus. *Neurobiol. Dis.* **63**, 229–236 (2014).
32. O. C. Meijer *et al.*, Penetration of dexamethasone into brain glucocorticoid targets is enhanced in mdr1A P-glycoprotein knockout mice. *Endocrinology* **139**, 1789–1793 (1998).
33. S. Mori, P. Maher, B. Conti, Neuroimmunology of the Interleukins 13 and 4. *Brain Sci.* **6**, 18 (2016).
34. L. L. W. Wang *et al.*, Cell therapies in the clinic. *Bioeng. Transl. Med.* **6**, 1–36 (2021).
35. B. A. Durafour *et al.*, Comparison of polarization properties of human adult microglia and blood-derived macrophages. *Glia* **60**, 717–727 (2012).
36. O. Butovsky *et al.*, Induction and blockage of oligodendrogenesis by differently activated microglia in an animal model of multiple sclerosis. *J. Clin. Invest.* **116**, 905–915 (2006).
37. N. Schweingruber, S. D. Reichardt, F. Lühder, H. M. Reichardt, Mechanisms of glucocorticoids in the control of neuroinflammation. *J. Neuroendocrinol.* **24**, 174–182 (2012).
38. D. A. Joyce, J. H. Steer, L. J. Abraham, Glucocorticoid modulation of human monocyte/macrophage function: Control of TNF- α secretion. *Inflamm. Res.* **46**, 447–451 (1997).
39. E. Kamma, W. Lasisi, C. Libner, H. S. Ng, J. R. Plemel, Central nervous system macrophages in progressive multiple sclerosis: Relationship to neurodegeneration and therapeutics. *J. Neuroinflammation* **19**, 1–27 (2022).
40. Hooke Laboratories, MOG/CFA-Induced EAE in C57BL/6 Mice. <https://hookelabs.com/services/cro/ea/ea/MOGCFA-inducedEAEinC57BL6mice.html>. Accessed 2 April 2023.
41. G. Locatelli *et al.*, Mononuclear phagocytes locally specify and adapt their phenotype in a multiple sclerosis model. *Nat. Neurosci.* **21**, 1196–1208 (2018).
42. D. A. Giles *et al.*, Myeloid cell plasticity in the evolution of central nervous system autoimmunity. *Ann. Neurol.* **83**, 131–141 (2018).
43. D. Blumenthal, Pre-clinical development of CAR Monocytes (CAR Mono) for solid tumor immunotherapy (2022) (3 December 2022).
44. S. Kim *et al.*, Monocyte enrichment from leukapheresis products by using the Elutra cell separator. *Transfusion* **47**, 2290–2296 (2007), [10.1111/j.1537-2995.2007.01470.x](https://doi.org/10.1111/j.1537-2995.2007.01470.x).
45. A. Faradji *et al.*, Large scale isolation of human blood monocytes by continuous flow centrifugation leukapheresis and counterflow centrifugation elutriation for adoptive cellular immunotherapy in cancer patients. *J. Immunol. Methods* **174**, 297–309 (1994).
46. A. C. Anselmo *et al.*, Monocyte-mediated delivery of polymeric backpacks to inflamed tissues: a generalized strategy to deliver drugs to treat inflammation. *J. Control Release* **199**, 29–36 (2015).
47. N. L. Klyachko *et al.*, Macrophages with cellular backpacks for targeted drug delivery to the brain. *Biomaterials* **140**, 79–87 (2017).
48. C. W. Shields *et al.*, Cellular backpacks for macrophage immunotherapy. *Sci. Adv.* **6**, eaaz6579 (2020).
49. M. Wagner *et al.*, Isolation and intravenous injection of murine bone marrow derived monocytes. *J. Vis. Exp.*, **52347** (2014).
50. A. Francke, J. Herold, S. Weinert, R. H. Strasser, R. C. Braun-Dullaeus, Generation of mature murine monocytes from heterogeneous bone marrow and description of their properties. *J. Histochem. Cytochem.* **59**, 813 (2011).
51. Hooke, Protocols - EAE induction by active immunization in C57BL/6 mice (2022) (4 March 2023).
52. S. M. Agrawal, C. Silva, W. W. Tourtellotte, V. W. Yong, EMMPRIN: A novel regulator of leukocyte transmigration into the CNS in multiple sclerosis and experimental autoimmune encephalomyelitis. *J. Neurosci.* **31**, 669–677 (2011).
53. G. Casella *et al.*, Oligodendrocyte-derived extracellular vesicles as antigen-specific therapy for autoimmune neuroinflammation in mice. *Sci. Transl. Med.* **12**, eaba0599 (2020).
54. P. Bankhead *et al.*, QuPath: Open source software for digital pathology image analysis. *Sci. Rep.* **7**, 16878 (2017).